BNL-224859-2023-TECH

EIC-ADD-TN-071

Updates on the Wake Potential Calculations for the Electron-ion Collider with ECHO3D

G. Wang

September 2023

Electron-Ion Collider

Brookhaven National Laboratory

U.S. Department of Energy

USDOE Office of Science (SC), Nuclear Physics (NP) (SC-26)

DISCLAIMER

Updates on the Wake Potential Calculations for the Electron-ion Collider with ECHO3D

G. Wang, A. Blednykh, M. Sangroula and S. Verdú-Andrés

Abstract

ECHO3D has been used for calculating the geometric impedance and short-range wakefields for several EIC (Electron-Ion Collider) beamline vacuum components in the past few years [1]. This note summarizes the wake potential calculations conducted in 2023 with ECHO3D for components from both the hadron storage ring (HSR) and the electron storage ring (ESR). For the HSR, calculations have been carried out for the polarimeter, the beam screen with pump slots and the bellow with pump ports. For the ESR, the short-range wake potential for the flange weld as well as various designs of the storage ring cavity have been calculated.

Calculation of the Wake Potential for the HSR

1. HSR beam screen with pumping slots

For reduced beam-induced resistive wall heating and to suppress electron cloud buildup, a copper-coated stainless steel beam screen chamber with a thin film of amorphous carbon will be installed in the beamline of the superconducting magnets of RHIC used for the HSR [2]. A section of the screen is shown in Fig. 1. There are four rows of pumping slots on both upper and lower walls of the screen. The length of the pumping slot is 17 mm and the width is 2 mm. The longitudinal separation of two adjacent slots is 18 mm. The total length of the considered model is 50 cm.

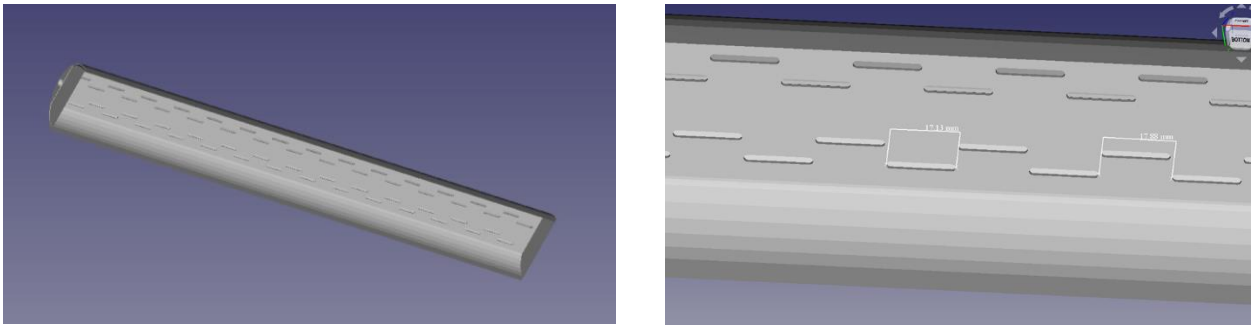

Figure 1: 3D model of the beam screen to be installed in the HSR.

The shortest proton bunches in the HSR have a rms bunch length of 60 mm. To compute the pseudo-Green function, a pilot bunch with an rms length of 4 mm is used. The longitudinal wake potential computed by three different codes, CST [3], ECHO3D [4] and GdfidL [5], is shown in Fig. 2. The short-range wake potential obtained from ECHO3D and GdfidL are in good agreement. However, the longitudinal wake potential calculated by CST is significantly different from that calculated by the other two codes, especially in the long range, as shown in the right plot of Fig. 2. The CST simulation is set to account for at least 50 modes in the port boundary to guarantee that reflections at the beam entry and exit are small [6]; however, the discrepancy with respect to the results provided by ECHO3D and GdfidL suggests that a convergence study to find the optimal number of modes is needed. Fig. 3 shows the longitudinal impedance calculated from the wake potential shown in Fig. 2. The impedance spectrum calculated from CST finds higher Q, narrower-band resonances than those from the other two codes, as one would expect from the different amplitude for long-range wake potential shown in Fig. 2 (right). Since the wake lengths used to compute

the impedance are not dramatically different, the discrepancy is not due to the resolution in frequency domain.

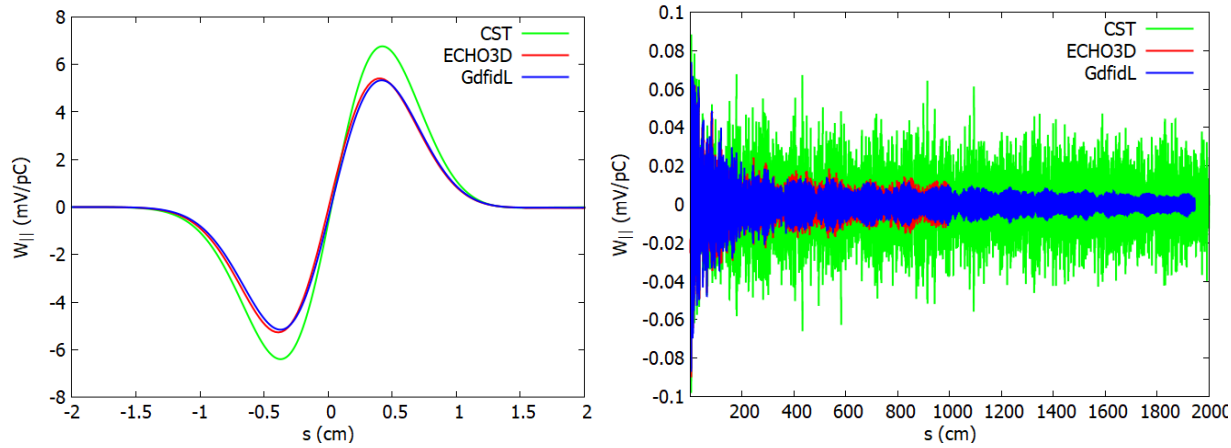

Figure 2: Longitudinal wake potential induced by a pilot proton bunch with R.M.S. bunch length of 4 mm as it passes through the beam screen shown in Fig. 1. The displayed wake potentials are obtained from CST (green), ECHO3D (red) and GdfidL (blue).

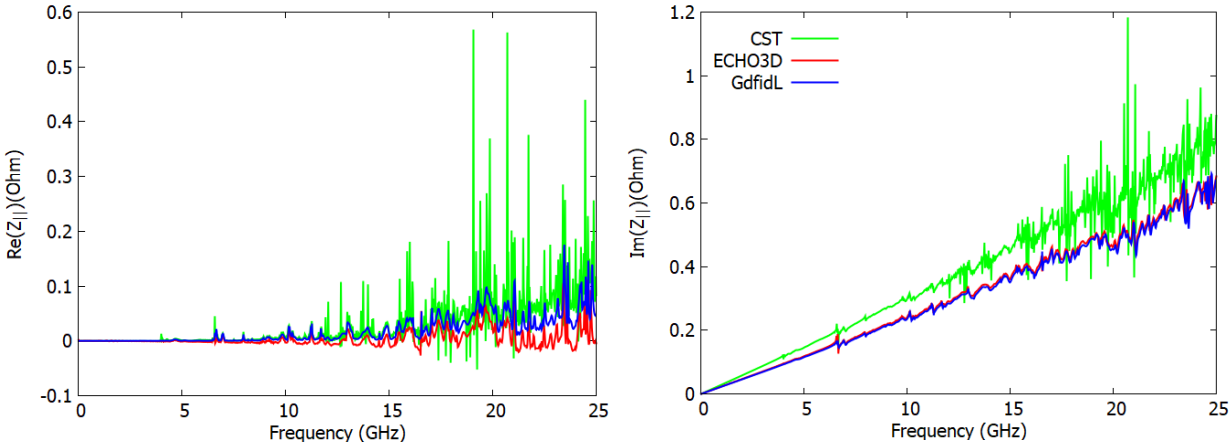

Figure 3: Longitudinal impedance of the beam screen with pumping slots as calculated from CST (green), ECHO3D (red) and GdfidL (blue). The wake length used for calculating the impedance is 20 meters for CST, 19.5 meters for GdfidL and 10 meters for ECHO3D.

2. HSR Polarimeter

Since EIC collides polarized particles, the polarimeter will be installed in the HSR to measure the polarization of the protons. For the wake potential calculation, the targets in the polarimeter has to be removed so that the beam can pass through for the calculation. The model of the polarimeter without the target is shown in fig. 4. Fig. 5 compares the longitudinal wake potential as calculated from ECHO3D and that calculated from CST, showing good agreements between results from the two codes.

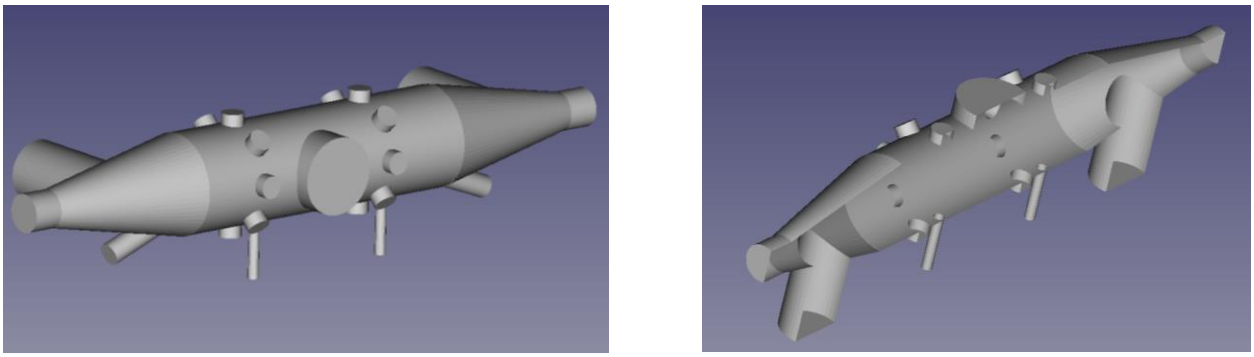

Figure 4: 3D model of the polarimeter. The target is removed to allow the beam passing through.

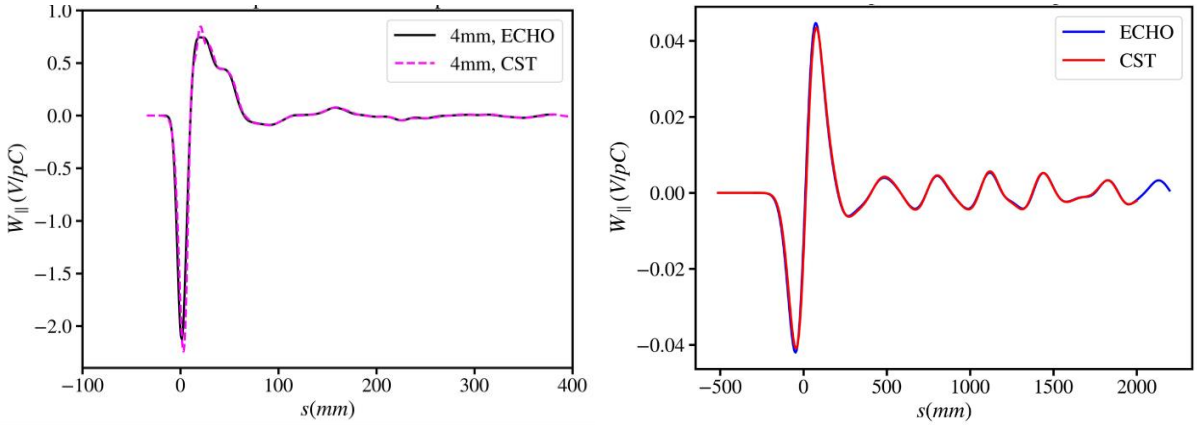

Figure 5: Comparison of the longitudinal wake potential as calculated from ECHO3D and that from CST. The left plot shows the longitudinal wake potential induced by a proton bunch with RMS bunch length of 4 mm and the right plot shows the wake potential induced by a bunch with 6 cm of RMS bunch length.

The short-range longitudinal wake potential for s< 20 cm does not converge well with the longitudinal range of the wake potential as shown in fig. 6 (left) and finer mesh may be needed to increase the total simulated range. However, for s >20 cm, it converges very well as shown in fig. 6 (right). Fig. 7 shows the longitudinal impedance as calculated from the wake potential.

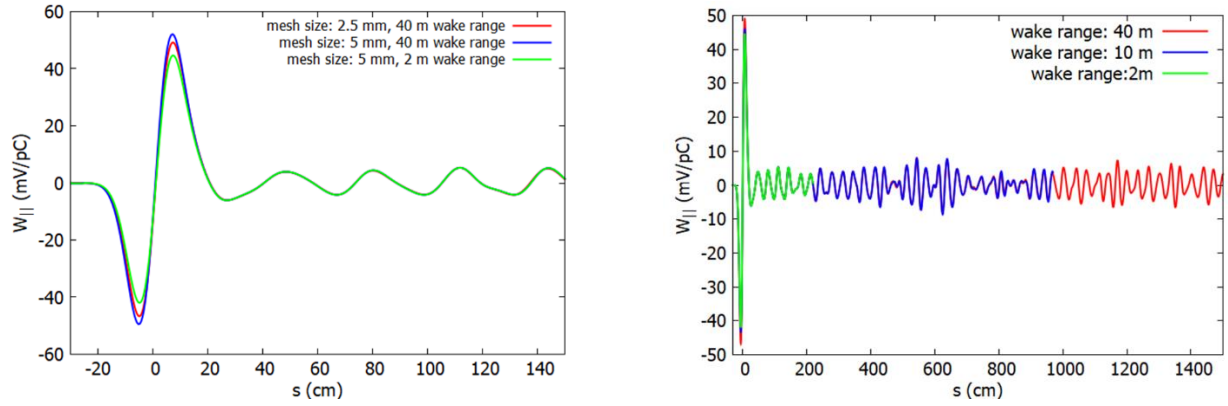

Figure 6: Study of the convergence of the longitudinal wake potential with the simulated range.

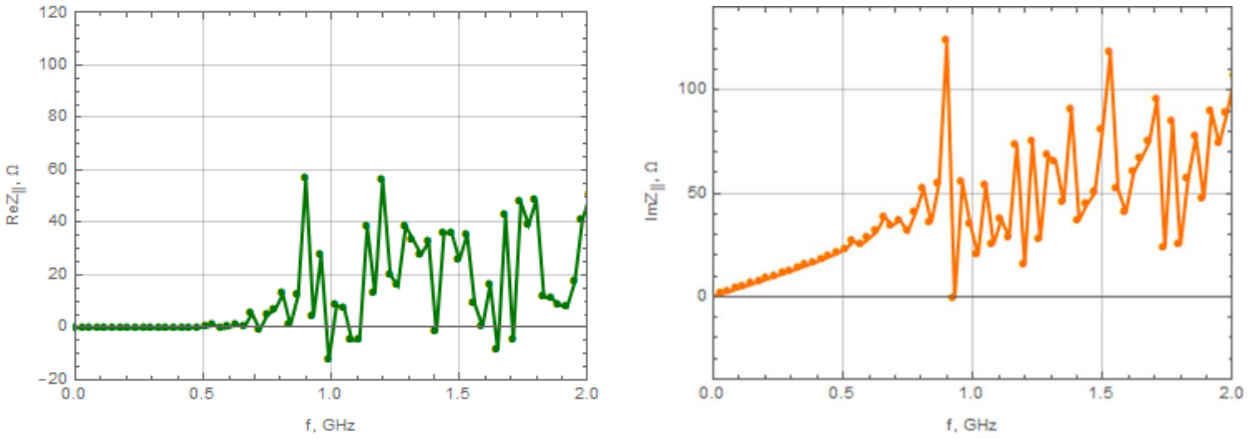

Figure 7: The longitudinal impedance calculated from the wake potential as shown in fig. 6 for the HSR polarimeter. The wake potential with 10 m longitudinal range was used in calculating the wake potential.

3. HSR Bellows with pump ports

The bellow is used to connect two pieces of the vacuum chamber in the HSR. The simplified model used for the wake potential simulation is shown in fig. 8.

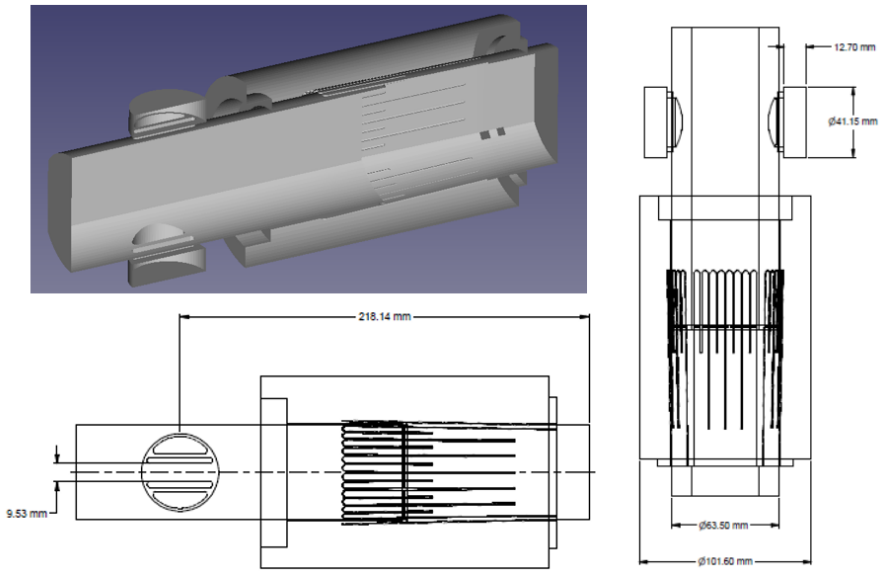

Figure 8: Model of the HSR bellow used in the wake potential simulation.

Fig. 9 shows that the longitudinal wake potential as calculated from ECHO3D and GdfidL have good agreement and the results from ECHO3D are converging for different step size. Fig. 10 shows the longitudinal wake potential for longer range. The longitudinal impedance calculated from the wake potential is shown in fig. 11 and spikes with ~5.5 GHz separation are observed from the impedance spectrum.

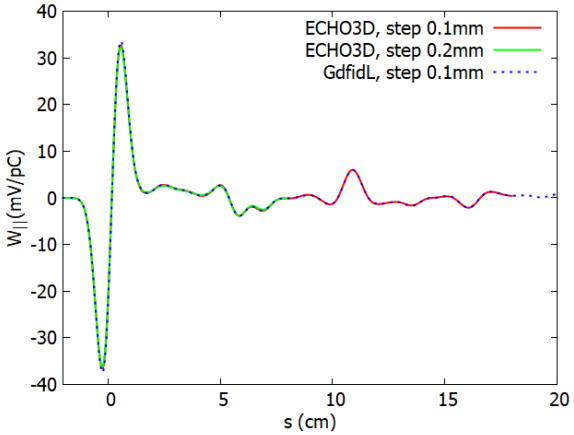

Figure 9: Comparison of the short-range longitudinal wake potential as calculated with ECHO3D and GdfidL.

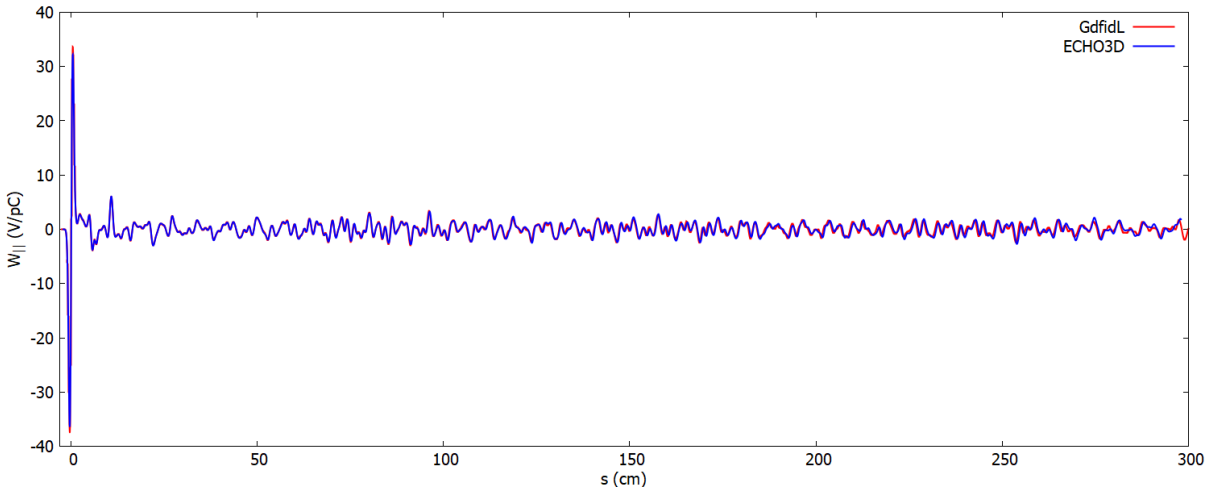

Figure 10: Comparison of the longitudinal wake potential as calculated with ECHO3D and GdfidL for wake range of 3 meters.

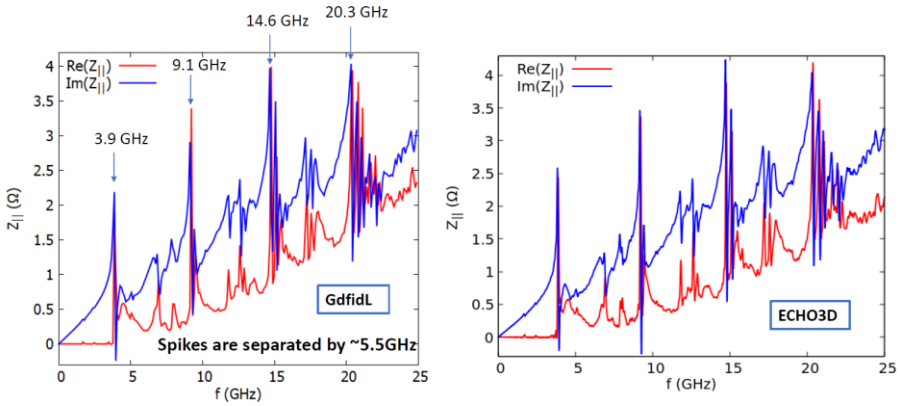

Figure 11: The longitudinal impedance as calculated from GdfidL (left) and ECHO3D (right) for the HSR bellow.

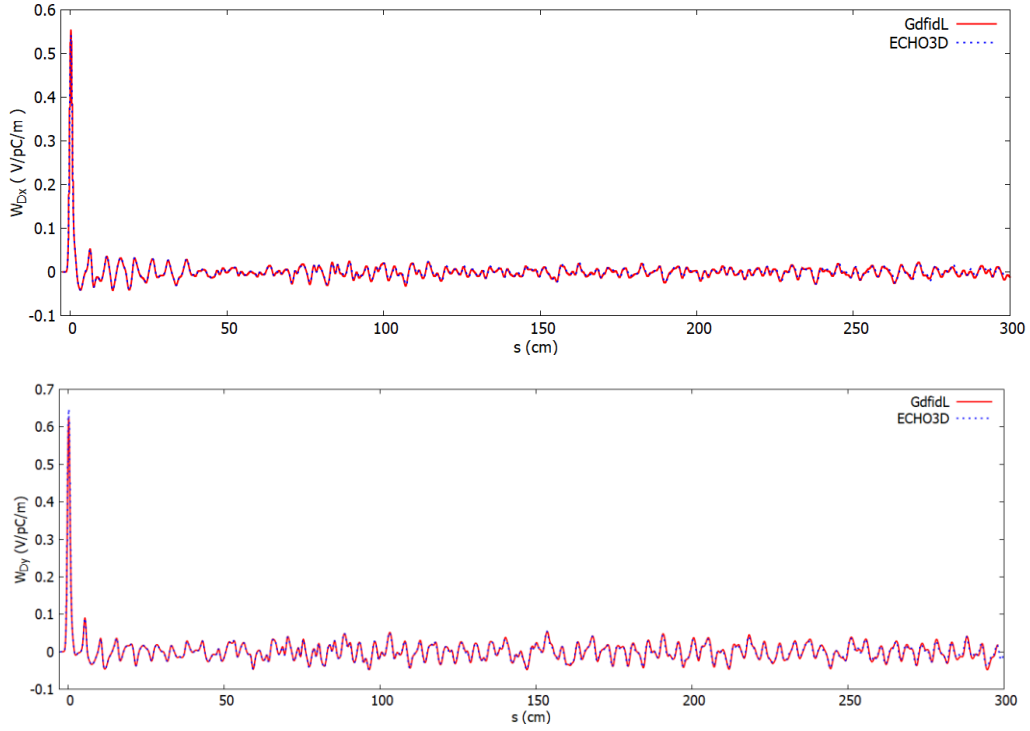

Figure 12: Comparison of the dipole horizontal wake potential (top) and dipole vertical wake potential (bottom) as calculated with ECHO3D and GdfidL for wake range of 3 meters.

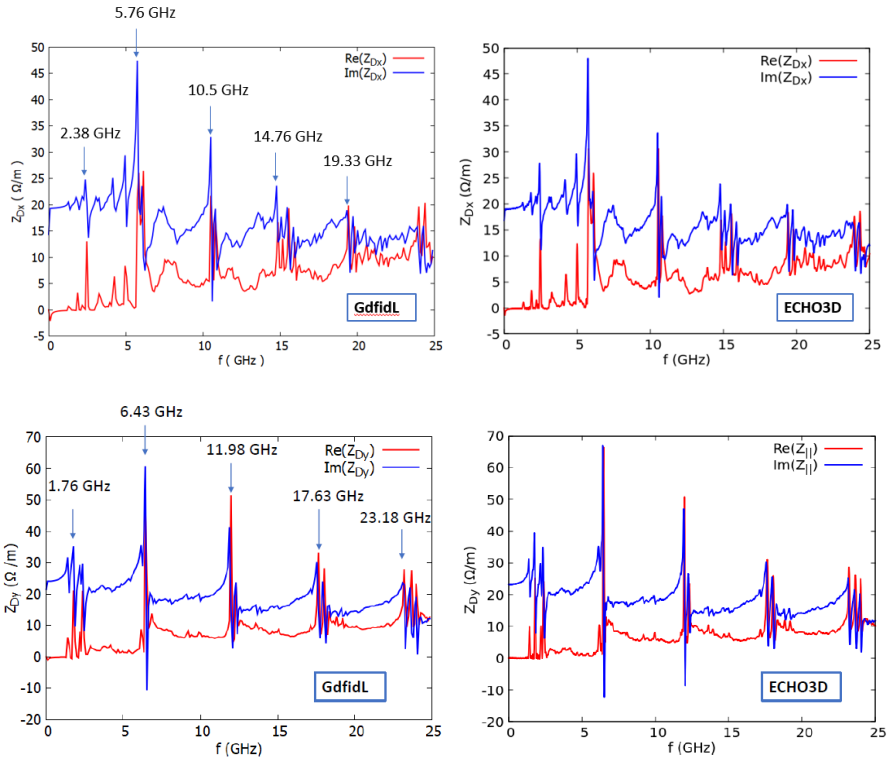

Figure 13: The horizontal (top) and vertical (bottom) dipole impedances as calculated from GdfidL (left) and ECHO3D (right) for the HSR bellow.

The horizontal and vertical dipole wake potential as calculated from the two codes also agree very well as shown in fig. 12. Fig. 13 shows the horizontal and vertical dipole impedance as calculated from the wake potential, which also has the spikes with ~5.5 GHz separation in the spectrum. One note about calculating the transverse dipole wake potential using the electric boundary condition at the mid-plane is that the exciting charge in the input file should be reduced by a factor of 2 in GdfidL if a symmetric boundary condition is used in the mid-plane to simulate half of the structure since the antisymmetric exciting charge density reads (Eq. (37) of Ref.[7])

$$\rho_m^{\,E}(y_0, y, s) = \frac{1}{2} Q\left[\delta(y - y_0) - \delta(y + y_0)\right]\lambda(s) \cdot$$

The vertical quadrupole wake potential was calculated by integrating the derivative of the longitudinal wake potential. Since calculating the derivative of the longitudinal wake potential along the vertical direction involves subtracting two large numbers, the accuracy of the quadrupole wake potential is problematic. Fig. 14 shows the vertical quadrupole wake potential, indicating significant discrepancies between the results obtained from the two codes, especially for s > 1.5 m. A similar problem was encountered when I was calculating the quadrupole wake potential for the ESR cavity. The author of ECHO3D was contacted and is looking into the issue.

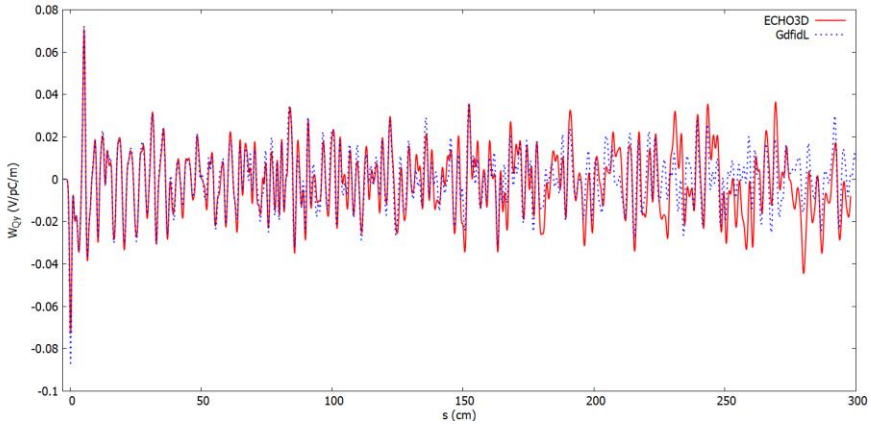

Figure 14: The quadrupole wake potential as calculated from ECHO3D and GdfidL.

The impedances as calculated from the two codes, however, share a lot of similarities, including the frequencies for the spikes and the amplitude of the spikes, as shown in fig. 15. It appears that the quadrupole wake potential as calculated by GdfidL is more accurate than those from ECHO3D, i.e. no noise like structures due to numerical errors introduced while subtracting two large numbers.

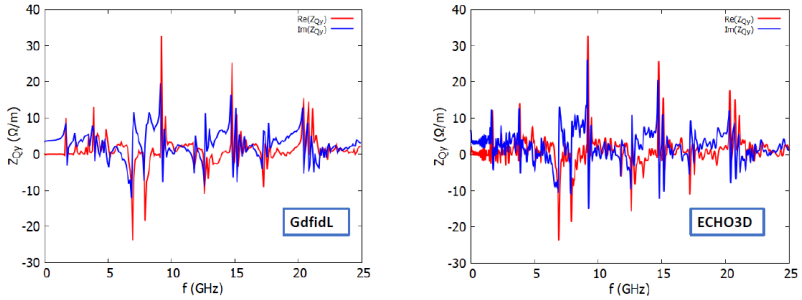

Figure 15: The quadrupole impedance as calculated from ECHO3D (right) and from GdfidL (left).

Calculation of the Wake Potential for the ESR

1. ESR 591 MHz Cavity

An asymmetric design of the ESR 591MHz cavity is currently under consideration. One side of the cavity has beam pipe with radius of 75 mm and the other side of the cavity has beam pipe radius of 173 mm. Compared with the previous symmetric design, the asymmetric design is more compact. The 3D model and its geometry are shown in fig. 16.

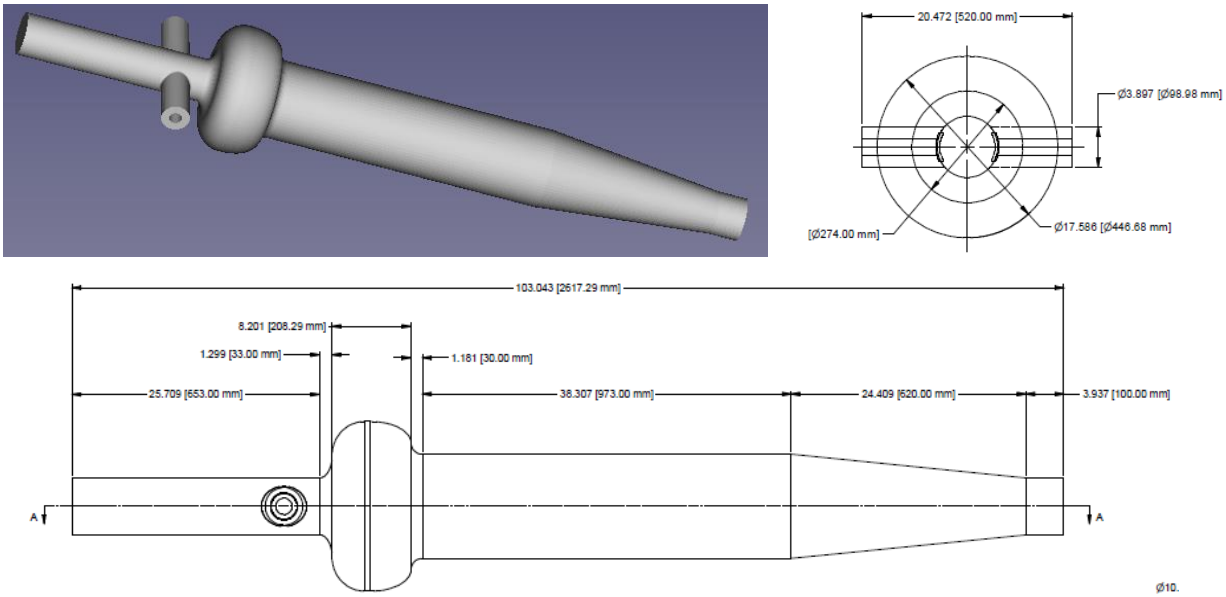

Figure 16: 3D model of the asymmetric design of the 591 MHz ESR storage ring cavity.

The longitudinal wake potential of the ESR cavity as shown in fig. 16 is shown in fig. 17 and the agreement between ECHO3D and GdfidL is reasonable.

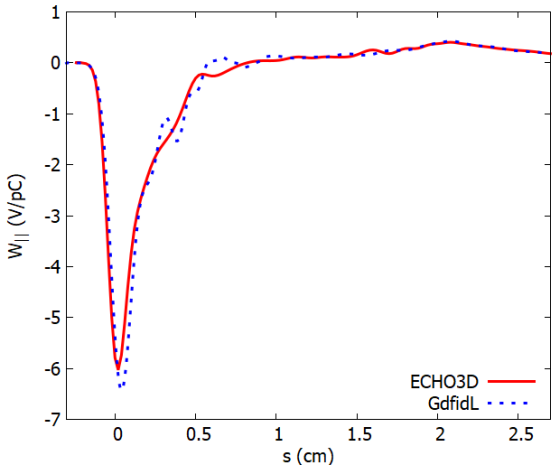

Figure 17: The longitudinal wake potential as calculated by ECHO3D and GdfidL.

However, the quadrupole wake potential calculated from ECHO3D does not converge with the transverse offset used to calculate the derivative of the longitudinal wake potential (see fig. 18). Since the transverse

wake potential is derived by integrating the derivative of the longitudinal wake potential, the longitudinal wake potential should be accurate enough to get the correct derivatives. As mentioned previously, the problem with this issue is still under investigation.

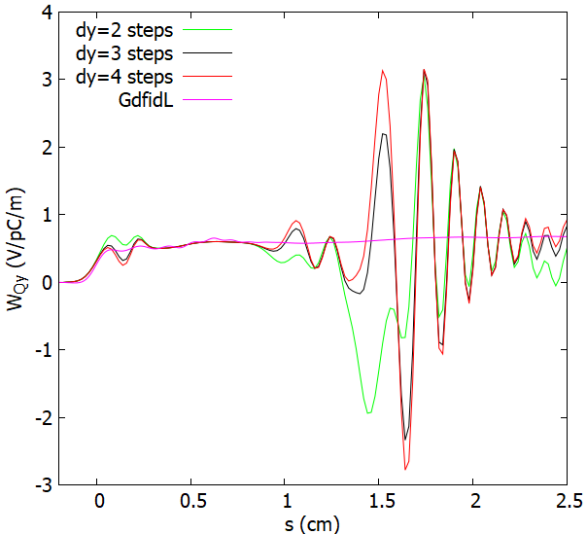

Figure 18: Vertical quadrupole wake potential calculated with different offset, dy, are significantly different from each other, suggesting that the longitudinal wake potential is not calculated correctly across the transverse plane.

The beam pipe needs to be tapered down to 36 mm on both sides of the ESR storage ring cavity. In order to choose the proper taper ratio, the impedances have been calculated for two models with different taper ratio, 6:1 and 10:1, as shown in fig. 19 and fig. 20.

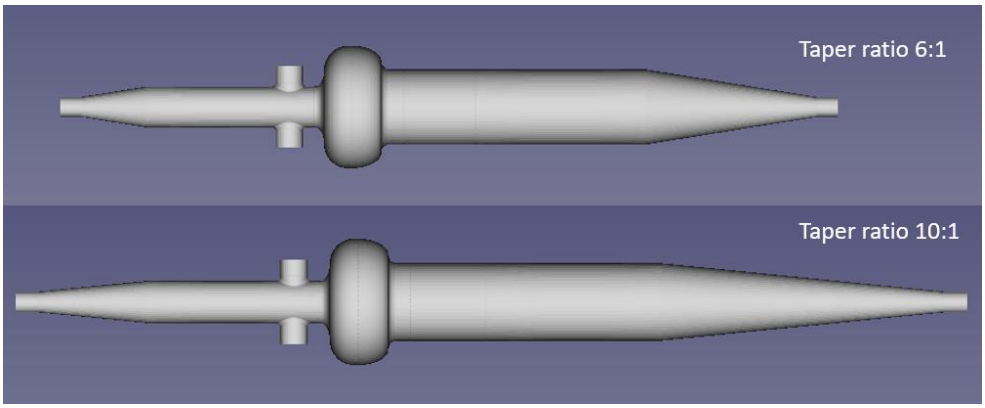

Figure 19: 3D models of the ESR 591 MHz cavity with tapered beam pipe transition.

As a first step, ECHO1D was used to simulate the wake potential. Since only structures with axial symmetry are allowed in ECHOz1 and ECHOz2, the simulated structure does not have the ports and the geometry used in ECHOz1 is shown in fig. 21.

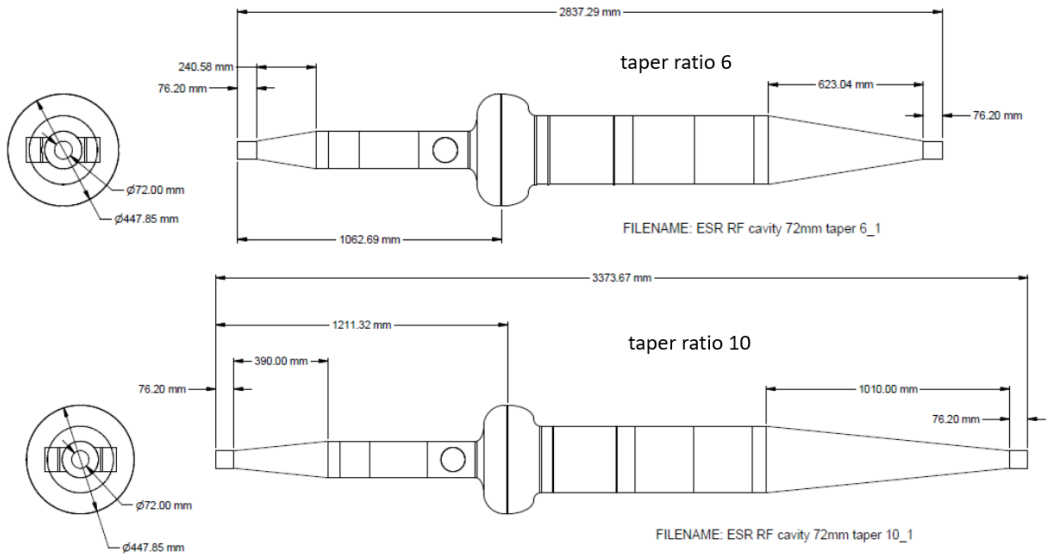

Figure 20: drawings of the ESR cavity with tapered transition.

The results from the ECHO1D simulation, with 0.5 mm of RMS bunch length, are shown in fig. 4 which shows that there is no significant reduction in the wake potential as a result of increasing the taper ratio from 6 to 10.

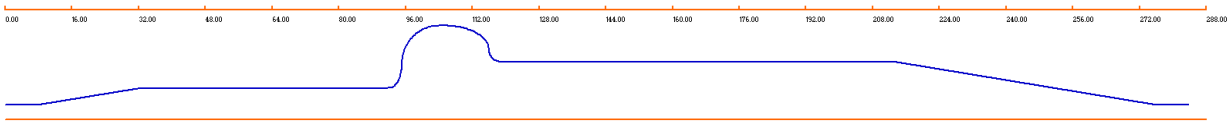

Figure 21: Geometry applied in ECHO1D simulation for the ESR cavity.

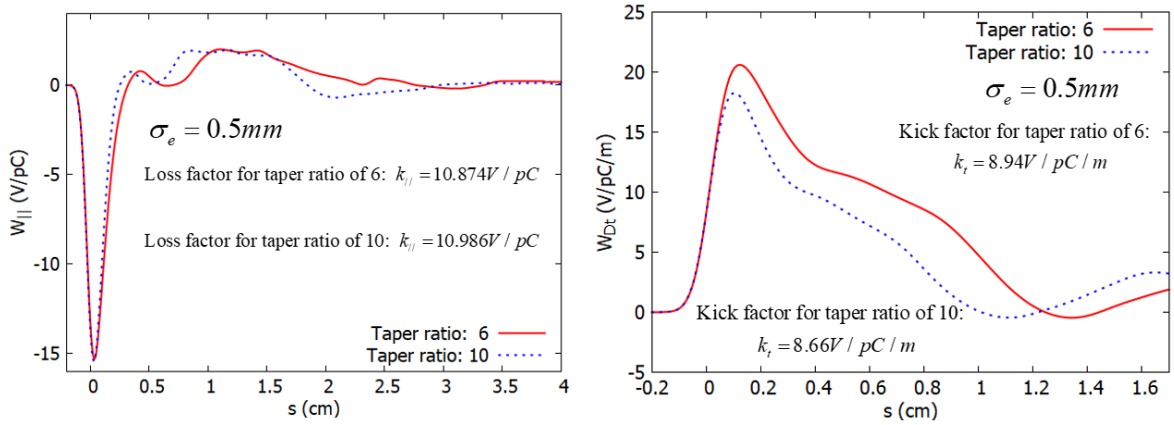

Figure 22: The longitudinal wake potential (Left) and the transverse dipole wake potential (Right) as calculated from ECHOz1 and ECHOz2.

ECHO3D was used to simulate the 3D model with ports and the results are shown in fig. 23, which do not differ significantly from the results shown in fig. 22 as obtained from ECHOz1 and ECHOz2. Fig. 24 shows the comparison between the results from ECHO1D and ECHO3D, indicating that the contribution from the ports that are missing from ECHO1D simulation is small compared to the rest of the structure.

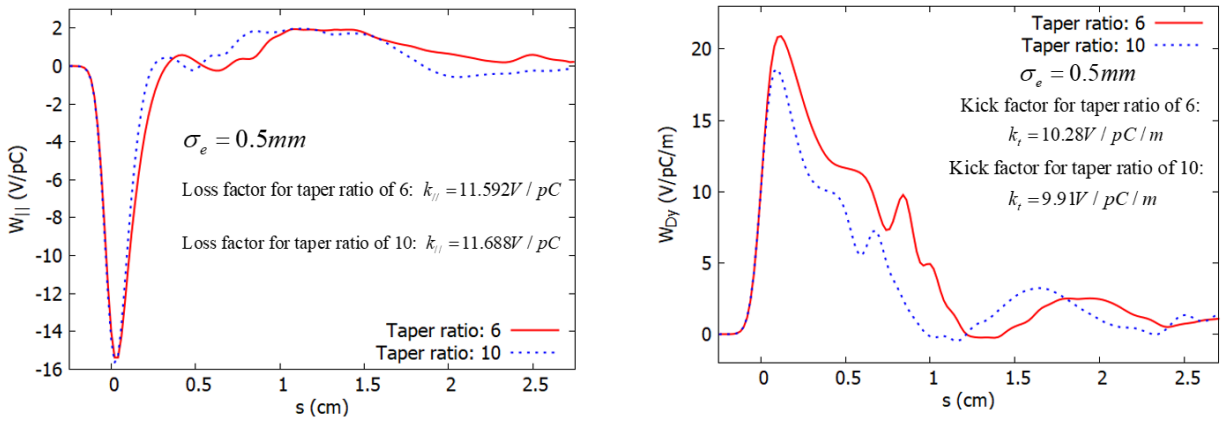

Figure 23: The longitudinal wake potential (left) and the transverse dipole wake potential (right) as calculated from ECHO3D.

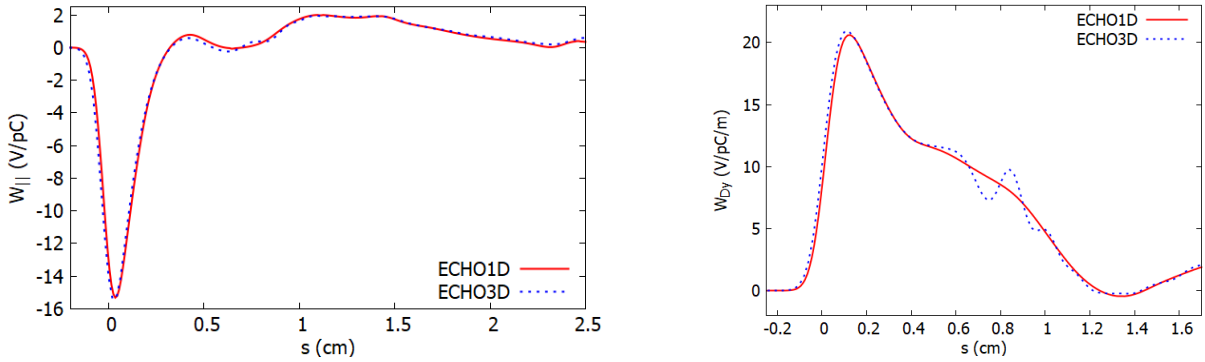

Figure 24: Comparison of the longitudinal wake potential (Left) and the transverse dipole wake potential (Right) from ECHO1D with that from ECHO3D for the structure with taper ratio 6.

From the results from ECHO1D and ECHO3D, with RMS bunch length of 0.5 mm (ESR Pseudo Green Function), it appears that increasing the taper ratio from 6 to 10 will only reduce the loss factor and kick factor by a few percent.

The intention of using 0.5 mm for calculating wake potential is to get information about the single bunch instability, i.e. the wake potential serves as a pseudo-Green function. In order to see the effectiveness of increasing the taper ratio, simulations have been repeated for 6 mm of RMS bunch length.

For the bunch length of 6 mm, ECHO1D simulation is converging with mesh size of 0.5 mm as shown in fig. 25. The comparison of the wake potentials for taper ratio of 6 and the taper ratio of 10 are shown in fig. 26. As shown in fig. 26, increasing the taper ratio from 6 to 10 reduces the loss factor by 23% and the kick factor by 26%, which is much more significant than what is observed for RMS bunch length of 0.5mm as shown in fig. 22.

Fig. 27 shows the results of ECHO3D with RMS bunch length of 6 mm for the wake field induced in the ESR cavity. The results from ECHO3D are almost identical to that from ECHO1D as shown in fig. 28.

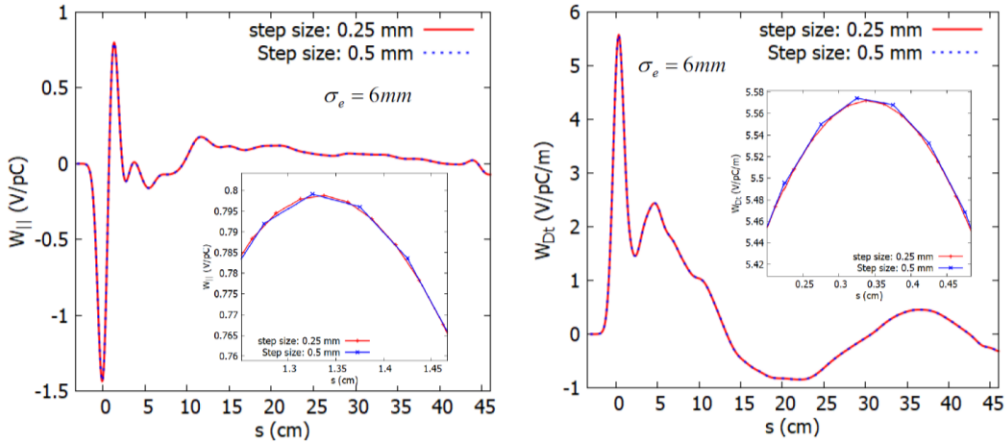

Figure 25: Convergences study of the longitudinal and transverse wake potential for ECHO1D simulation with RMS bunch length of 6mm. The taper ratio is 10 for this study.

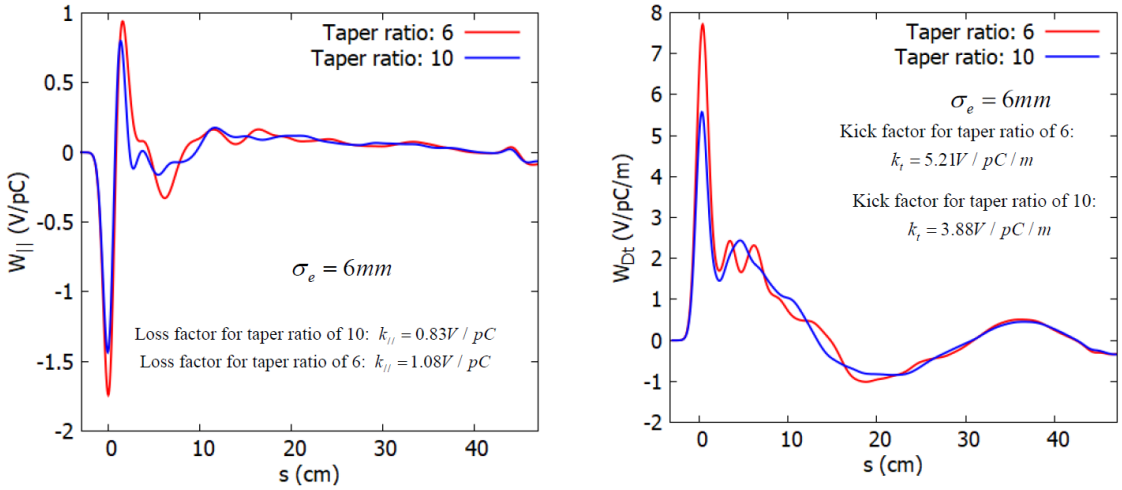

Figure 26: The longitudinal wake potential (left) and the transverse dipole wake potential (right) as calculated from ECHO1D with 6 mm of RMS bunch length.

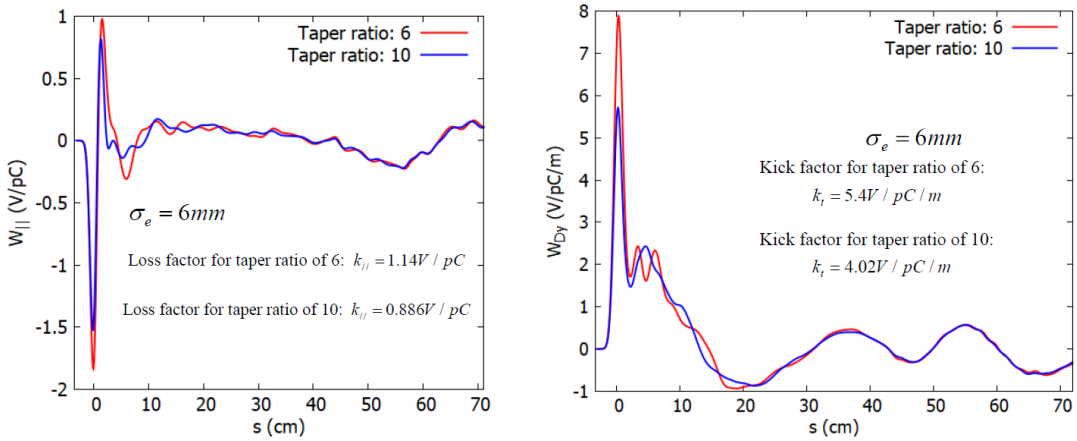

Figure 27: The longitudinal wake potential (left) and the transverse dipole wake potential (right) as calculated from ECHO3D with 6 mm of RMS bunch length.

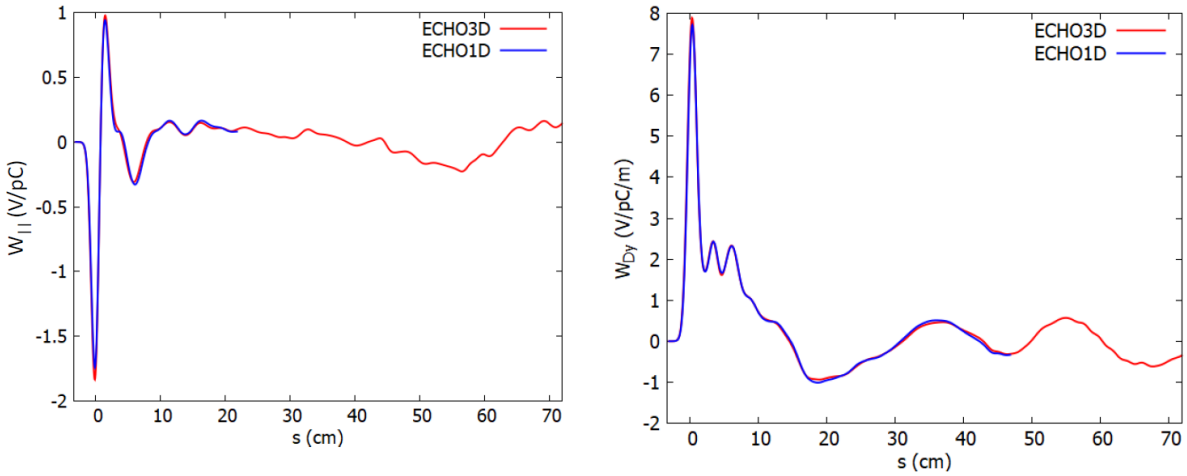

Figure 28: Comparison of the longitudinal wake potential (Left) and the transverse dipole wake potential (Right) from ECHO1D with that from ECHO3D for the structure with taper ratio 6.

2. The ESR flange weld step

In a design for welding the flanges of the ESR, a gap of 10 micrometers wide is expected and its contribution to the short-range wake field needs to be calculated. The geometry of the welding step is shown in fig. 29. Since the 10 micrometers gap in the geometry, the simulation steps should not be larger than 10 micrometers which make the ECHO3D simulation RAM consuming. ECHO2D simulation with the geometry shown in fig. 30 has been performed to benchmark the results of ECHO3D.

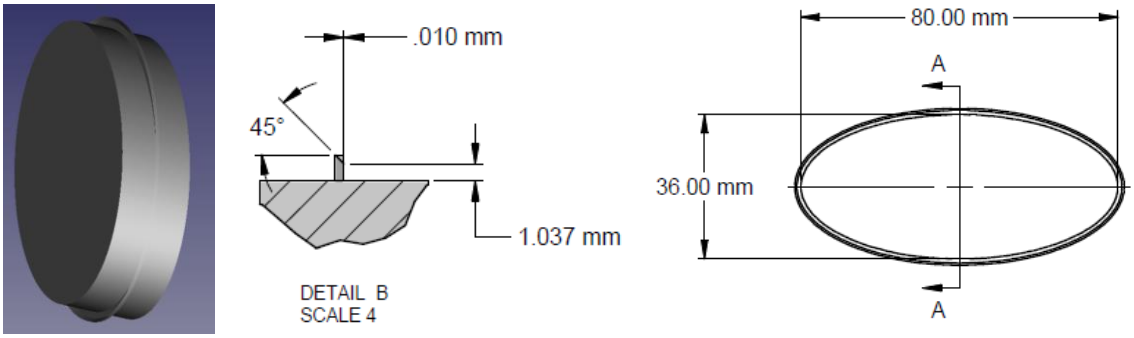

Figure 29: Geometry used for ECHO2D simulation of the ESR flange weld step.

The results for the longitudinal wake potential are shown in fig. 6, indicating that the 2D geometry with circular cross-section shares a lot of similarities with that of the 3D geometry with elliptical cross-section.

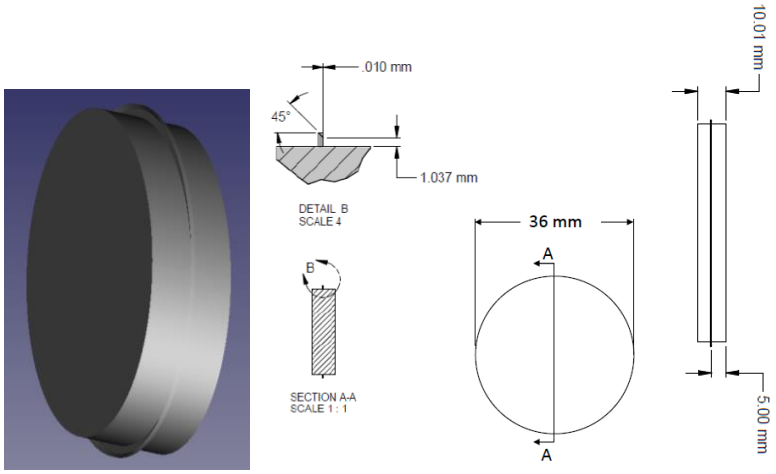

Figure 30: Geometry used for ECHO3D simulation of the ESR flange weld step.

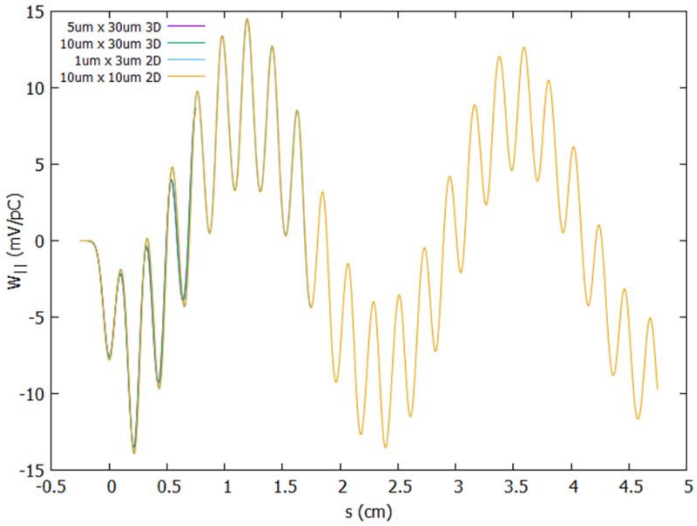

Figure 31: The longitudinal wake potential as calculated for the ESR flange weld step. The 3D results are for the geometry with elliptical beam pipe and the 2D results are for the 2D geometry with circular pipe as shown in fig. 30.

Summary

ECHO1D, ECHO2D and ECHO3D codes have been used in evaluating the short-range wakefields of the EIC vacuum components both in the HSR and ESR. It proves to be useful for benchmarking results obtained from other codes such as CST and GdfidL. Significant discrepancies among results from CST, ECHO3D and GdfidL have been identified through these studies for the HSR beam screen. While ECHO3D results are in good agreement with GdfidL, they are substantially different from what were obtained with CST, especially for longer range. The impedance from ECHO3D and GdfidL is also lack of the narrow spikes (with similar wake range as used for CST, i.e. 20 m) as observed from CST simulations, which requires further investigation.

During these studies, some problems with calculating of the quadrupole wake potential using ECHO3D have been identified and are under investigation.

REFERENCES

[1] G. Wang, M. Blaskiewicz, A. Blednykh, and M. Sangroula, in *12th International Particle Accelerator Conference (IPAC'21), Campinas, SP, Brazil, 24-28 May 2021* (2021), pp. 2675.

[2] S. Verdú-Andrés et al., Impedance considerations for the HSR beam screen design (under preparation).

[3] CST Particle Studio, www.cst.com.

[4] ECHO3D, echo4d.de.

[5] GdfidL, www.gdfidl.de.

[6] U. Niedermayer and E. Gjonaj, Wake field and bewam coupling impedance simulations, *ICFA Beam Dyn. Newslett.* 69 (2016) 78-87..

[7] I. Zagorodnov, K. Bane, and G. Stupakov, Physical Review Special Topics-Accelerators **18**, 104401 (2015).